# A Swine Model of Selective Geographic Atrophy of Outer Retinal Layers Mimicking Atrophic AMD: A Phase I Escalating Dose of Subretinal Sodium Iodate

Jordi Monés,[1–3] Marta Leiva,[4,5] Teresa Peña,[4,5] Gema Martínez,[3,6] Marc Biarnés,[1,2] Miriam Garcia,[1,2] Anna Serrano,[2] and Eduardo Fernandez[3,6]

[1]Barcelona Macula Foundation: Research for Vision, Barcelona Spain
[2]Institut de la Màcula, Centro Médico Teknon, Barcelona, Spain
[3]Networking Research Centre of Bioengineering, Biomaterials and Nanomedicine (CIBER-BBN), Madrid, Spain
[4]Departament de Medicina i Cirurgia Animals, Facultat de Veterinària, Universitat Autònoma de Barcelona, Barcelona, Spain
[5]Fundació Hospital Clínic Veterinari, Campus Universitat Autònoma de Barcelona, Barcelona, Spain
[6]Institute of Bioengineering, Universidad Miguel Hernández, Alicante, Spain

Correspondence: Jordi Monés, c/ Horaci 43, Barcelona, 08022, Spain; jmones@institutmacula.com.

Submitted: February 16, 2016
Accepted: June 13, 2016

Citation: Monés J, Leiva M, Peña T, et al. A swine model of selective geographic atrophy of outer retinal layers mimicking atrophic AMD: a phase I escalating dose of subretinal sodium iodate. *Invest Ophthalmol Vis Sci*. 2016;57:3974–3983. DOI:10.1167/iovs.16-19355

**Purpose.** To establish the dose of subretinal sodium iodate ($NaIO_3$) in order to create a toxin-induced large animal model of selective circumscribed atrophy of outer retinal layers, the retinal pigment epithelium (RPE), and photoreceptors, by spectral-domain optical coherence tomography (SD-OCT) and immunocytochemistry.

**Methods.** Fifteen male and female healthy Yorkshire pigs received unilateral subretinal escalating doses of $NaIO_3$ under general anesthesia. In all the animals, volumes of 0.1 to 0.2 mL $NaIO_3$ were injected into the subretinal space of the area centralis through a 23/38-gauge subretinal cannula. Control SD-OCTs were performed 1 and 2 months after the surgery, at which time pigs were euthanized and eyes enucleated. Globes were routinely processed for histologic and immunohistochemical evaluation.

**Results.** Spectral-domain OCT and immunohistochemistry revealed circumscribed and well-demarcated funduscopic lesions, limited to the outer retinal layers in pigs treated with 0.01 mg/mL subretinal sodium iodate.

**Conclusions.** The swine model of a controlled area of circumscribed retinal damage, with well-delimited borders, and selectively of the outer layers of the retina presented herein shows several clinical and histologic features of geographic atrophy in AMD. Therefore, it may represent a valuable tool in the investigation of new emerging regenerative therapies that aim to restore visual function, such as stem cell transplantation or optogenetics.

Keywords: geographic atrophy, age-related macular degeneration, animal models

**Objetivo.** Establecer la dosis de yodato de sodio ($NaIO_3$) subretiniano para crear un modelo en gran animal inducido por toxicidad de atrofia localizada en las capas externas de la retina, el epitelio pigmentario de la retina y los fotorreceptores, verificado mediante tomografía de coherencia óptica (SD OCT) e inmunohistoquímica.

**Métodos.** Quince cerdos sanos de raza Yorkshire de ambos sexos recibieron dosis escaladas unilaterales subretinianas de $NaIO_3$ bajo anestesia general. En todos los casos, volúmenes de 0.1 a 0.2ml de $NaIO_3$ se inyectaron en el espacio subretiniano del área centralis mediante una cánula subretiniana de 23/28G. Se realizaron tomografías al mes y a los 2 meses de la cirugía, momento en el que se practicó la eutanasia y enucleación. Los globos oculares se procesaron para evaluación histológica e inmunohistoquímica.

**Resultados.** El SD OCT y la inmunohistoquímica revelaron lesiones fundoscópicas bien delimitadas, circunscritas a las capas retinianas externas en cerdos tratados mediante 0.01 mg/ml de NaIO3 subretiniano.

**Conclusiones.** El modelo de cerdo con atrofia selectiva de la retina externa presentó muchas de las características clínicas e histológicas de la atrofia geográfica secundaria a degeneración macular. Por tanto, puede representar una herramienta útil en la investigación de nuevas terapias regenerativas cuyo objetivo es recuperar la función visual, como el trasplante de células madre o la optogenética.

Investigative Ophthalmology & Visual Science

Despite recent advances in treatment of the wet form of AMD,[1–6] the clinical outcome of AMD often remains blindness. Nowadays, the great challenge to which the ophthalmologic community is committed lies in finding a treatment that may slow the relentless progression of the atrophic form of the disease, together with other approaches that restore or regenerate the involved part of the diseased retinal tissue. Nowadays, the advanced form of dry AMD with geographic atrophy (GA) may be the first cause of legal blindness among elderly patients in the industrialized world, and it represents up to a third of cases of late AMD.[7,8] Besides the impact of the disease among individuals, the economic burden of atrophic AMD (drusen, RPE abnormalities, and/or GA) in the United States is enormous: $26,100 million annually in one study[9] and approximately 0.22% of its gross domestic product in 2010 in terms of wage loss from untreated disease in another report.[10]

The clinical presentation of dry AMD includes drusen, hyperplasia of the RPE. Geographic atrophy refers to confluent areas of RPE cell death accompanied by overlying photoreceptor atrophy. These areas are also characterized by diffuse and irregular patches of increased autofluorescence, which precede the development and enlargement of GA.[11] The likelihood of GA increases with age,[12,13] and its incidence is higher than that of wet AMD in individuals aged 85 years or older.[7] Therefore, the predicted increase in life expectancy may be accompanied by a greater prevalence of GA, especially in the older age group, resulting in a real epidemic burden in developed countries. Previous epidemiologic studies attributed approximately 20% of cases of severe visual loss to GA,[14] but given that the efficacy of antiangiogenic therapy is decreasing the rate of visual loss in wet AMD, this percentage possibly underestimates the current relative impact of GA in AMD. Additionally, results from the Comparison of AMD Treatments Trial suggest that antiangiogenic therapy for wet AMD may increase the spread of atrophy, which highlights the need to understand GA.[15] At present, no approved treatment for this condition exists.

In many patients, GA tends to spread around fixation, preserving the fovea until late in the course of the disease (so-called foveal sparing).[16,17] The reasons for this are unclear, although rods, whose density is highest in the perifoveal area, have been shown to be more sensitive to damage caused by AMD than cones.[18,19] Results from histologic[20,21] and psychophysical[22,23] studies have confirmed that rods are damaged earlier, and more severely, than cones in dry AMD and in aging.

Enormous progress has been made in the field of pathogenesis of AMD. However, it is still an extremely complex disease with many unresolved questions. Although extensive research and evidence of the role of oxidative stress, inflammation, and genetics on the pathogenesis of AMD have been provided, there is still no current treatment for GA forms.

Accurate animal models of a disease can assist greatly in the development of new therapies. The multifactorial nature of AMD has made the development of an animal model a challenging task,[24] and many different models of AMD have been created in mice, rats, rabbits, pigs, and nonhuman primates.[25] However, there is no animal model available that fully replicates all the features of AMD seen in humans.[26] After the primates, the retina of swine bears the closest resemblance to the human one. The advantages of the porcine model are the holangiotic retinal vasculature, the choroidal blood flow, the absence of tapetum, and the presence of a narrow horizontal retinal area, rich in cones, called area centralis, which mimics the human macula.[27] Moreover, the structure of the swine retina is very similar to the human one; the attachment between the RPE and Bruch's membrane is mediated by the interaction between integrins,[28] and their cone/rod ratio resembles the human ratio.[29]

Sodium iodate ($NaIO_3$) has been the most widespread retinotoxin used up to now to induce retinal degeneration resembling GA in animal models.[30] Systemic administration of $NaIO_3$ in mice, with doses ranging from 20 to 40 mg/mL, is known to selectively impair the RPE, resulting in patchy loss of RPE and subsequent degeneration of photoreceptors.[31] When it was used intravenously in a mouse model, the extent of RPE damage was dependent on the concentration of $NaIO_3$ and the time elapsed after injection.[32] The intravenous use of $NaIO_3$ in rats causes the coexistence of atrophic and preserved areas of RPE and choriocapillaris throughout the retina.[33] On the other hand, attempts to use intravenous $NaIO_3$ in pigs have failed to cause retinal damage at sublethal doses, below 110 mg/kg.[34]

The precise mechanism of toxicity is still unclear, although inhibition of lysosomal enzymes may play an important pathogenic role.[35] However, this model does not reproduce a controlled mechanism of anticipated and predetermined areas of highly distinct lesions, with clear borders between the relatively healthy retina outside the area of atrophy and the atrophy itself, as in patients with GA in advanced AMD. The inconvenience of current models of diffuse atrophy lies in the fact that there is no residual or remaining healthy host tissue that may help the new implanted tissue or cells to integrate and survive.

The purpose of this research study was to develop, in large animals, a model of areas of circumscribed atrophy with selective damage only of the outer retinal layers, and with healthy full-thickness retina remaining in their vicinity as in human atrophic AMD. This swine model of circumscribed selective atrophy of outer retinal layers may represent an advance in the research in regenerative medicine with stem cells or tissue transplant with a model closer to the GA secondary to AMD in humans, serving as proof of the concept of safety and efficacy of these aforementioned therapies in order to promote their phase I clinical trials in patients.

## Materials and Methods

### Animals

The experimental study was approved by the Institutional Animal Care and Use Committee of the Universitat Autónoma de Barcelona CEAAH 2180, and complied with the ARVO Statement for the Use of Animals in Ophthalmic and Vision Research. Fifteen healthy Yorkshire pigs of both sexes and 20- to 25-kg body weight were included in the study. Animals were provided by a Spanish Research Animal Resource Center and kept according to the national Animal Welfare legislation. Only pigs with complete bilateral ophthalmic examination were included in the study.

### $NaIO_3$ Preparation and Subretinal Injection

Starting from a theoretical intravenous 50 mg/kg (slightly above concentrations used in small animal models)[30,32] from a body weight of 20 kg, and an estimated blood total volume of 2 L, a solution of 0.5 mg/mL was calculated and obtained. Dilutions of 1/1000, 1/100, 1/10, and 1/1 were studied in seven pigs. Posteriorly, doses of ×2, ×10, and 1/20 and 1/50 were also evaluated in another group of eight pigs. Dilutions in distilled water were prepared at the chemistry lab of the Veterinary Faculty of the Universitat Autónoma de Barcelona.

All pigs were routinely premedicated and anesthetized. Premedication consisted of intramuscular injection of azaperone (Stressnil, 2 mg/kg; Laboratorios del Dr. Esteve, S. A., Barcelona, Spain) and ketamine (Imalgene, 15 mg/kg; Labo-

**Table 1.** List and Details of Antibodies Used in This Study

| Antibody | Antigen | Host | Source (Cat. No.) | Dilution | Target Cell Type |
|---|---|---|---|---|---|
| Claudin | Claudin-1 polyclonal antibody, C-18 | Goat | Santa Cruz* (sc-17658) | 1:100 | Retinal blood vessels |
| RPE65 | Anti-retinal pigment epithelium 65 antibody | Rabbit | Millipore† (AB5428) | 1:200 | Retinal pigment epithelium |
| Recoverin | Recombinant human recoverin | Rabbit | Millipore† (AB5585) | 1:400 | Rods and cones |
| Calbindin D-28K | Monoclonal antibody derived from 955 hybridoma | Mouse | Sigma-Aldrich Corp.‡ (C9848) | 1:300 | Horizontal cells |
| Calretinin | Rat calretinin | Goat | Millipore† (AB1550) | 1:300 | Amacrine and ganglion cells |

* Santa Cruz Biotechnology, Santa Cruz, California, USA
† Billerica, Massachusetts, USA
‡ St. Louis, Missouri, USA

ratorios Merial, Barcelona, Spain); and anesthetic induction was conducted by means of intravenous propofol (Propofol lipuro; B. Braun Medical SA, Barcelona, Spain). Pigs were intubated and maintained under general anesthesia with isoflurane 1.5% to 2% (Isoflo; Laboratorios del Dr. Esteve, S. A.) and 100% oxygen. Furthermore, all the animals received systemic parenteral antibiotics (5 mg/kg intramuscular, Ceftiofur, Naxcel; Pfizer SA, Madrid, Spain), as well as topical tropicamide (Colircusí tropicamida; Alcon Cusí Laboratories, Barcelona, Spain), tobramycin (Tobrex; Alcon Cusí Laboratories), and dexamethasone (Maxidex; Alcon Cusí Laboratories) as preoperative treatment.

The periocular skin of the right eyes was clipped and aseptically cleaned with povidone iodine solution (Braunol; B. Braun Vetcare S. A., Barcelona, Spain) diluted in 1:10 saline, and the corneal surface was cleansed with saline. The pig was positioned in lateral recumbency with the muzzle gently tilted.

Lateral canthotomy was performed in all the right eyes. Two 23-gauge vitrectomy trocars were inserted at 3 mm from the limbus, one for the intraocular light pipe and the other for the subretinal injection cannula (23/38 G; Medone Surgical; Sarasota, FL, USA). Neither vitrectomy nor posterior hyaloid manipulation was performed and no infusion was used. Volume of 0.1 to 0.2 mL of the selected dose of $NaIO_3$ was injected into the subretinal space between the retinal vessel arcades, at either the nasal or the temporal side of the optic disc. Canthotomy was performed and sutured at the end of the surgery (6/0, Vicryl; Ethicon, Somerville, NJ, USA).

## Postoperative Follow-Up

Anterior segment biomicroscopy (Kowa SL-15 Portable Slit Lamp Biomicroscope; Kowa Co. Ltd, Tokyo, Japan), tonometry (Tonovet; Icare, Oy, Finland), and indirect fundus ophthalmoscopy (Omega 180; Heine, Herrsching, Germany) were performed at 1 week, 1 month, and 2 months postoperatively.

Color fundus photography and spectral-domain optical coherence tomography (SD-OCT) using Spectralis HRA+OCT (Heidelberg Engineering, Heidelberg, Germany) were performed in both eyes at 1 month and 2 months after the surgery. Sedation was achieved by the above-mentioned

**Table 2.** Fundus and SD OCT Findings Related to the $NaIO_3$ Concentration Used

| Swine | $NaIO_3$, mg/mL | Indirect Ophthalmoscopy | SD-OCT |
|---|---|---|---|
| 1 | 0.0005 | No changes | No changes |
| 2 | 0.005 | No changes | No changes |
| 3 | 0.05 | Moderate pigmentary changes | Marked atrophy and thinning of all retinal layers, RPE not affected |
| 4 | 0.05 | Moderate pigmentary changes | Marked atrophy and thinning of all retinal layers, RPE not affected |
| 5 | 0.5 | Severe pigmentary changes | Marked atrophy and thinning of all retinal layers, RPE partially disrupted |
| 6 | 0.5 | Severe pigmentary changes | Marked atrophy and thinning of all retinal layers, RPE partially disrupted |
| 7 | 1 | Severe pigmentary changes | Marked atrophy and thinning of all retinal layers, RPE partially disrupted |
| 8 | 3 | Panuveitis | NA |
| 9 | 0.025 | Mild pigmentary changes | Selective atrophy of outer retinal layers including outer plexiform layer |
| 10 | 0.025 | Mild pigmentary changes | Selective atrophy of outer retinal layers including outer plexiform layer |
| 11 | 0.01 | Died | NA |
| 12 | 0.01 | Mild pigmentary changes | Selective thinning of the outer nuclear layer<br>Irregularities, discontinuities, and increased reflectivity of the 2 outer bands, interdigitation zone and RPE/Bruch's membrane, in addition to loss of the ellipsoid |
| 13 | 0.01 | Mild pigmentary changes | Selective thinning of the outer nuclear layer<br>Irregularities, discontinuities, and increased reflectivity of the 2 outer bands, interdigitation zone and RPE/Bruch's membrane, in addition to loss of the ellipsoid |
| 14 | 0.01 | Mild pigmentary changes | Selective thinning of the outer nuclear layer<br>Irregularities, discontinuities, and increased reflectivity of the 2 outer bands, interdigitation zone and RPE/Bruch's membrane, in addition to loss of the ellipsoid |
| 15 | 0.01 | Mild pigmentary changes | Selective thinning of the outer nuclear layer<br>Irregularities, discontinuities, and increased reflectivity of the 2 outer bands, interdigitation zone and RPE/Bruch's membrane, in addition to loss of the ellipsoid |

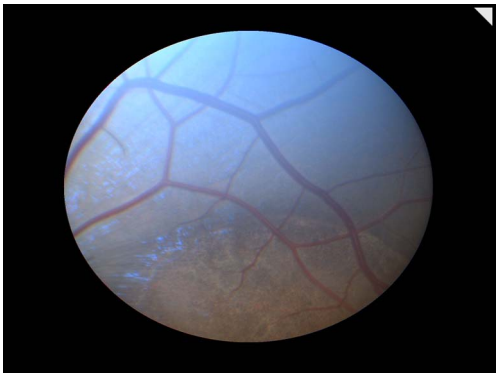

FIGURE 1. Fundus color photography at 1 month after subretinal administration of 0.1 mL $NaIO_3$ at concentration of 0.05 mg/mL in pig 3. A well-demarcated round area of pigmentary changes is observed at the area where the bleb was created. No retinal findings are visible.

protocol. Briefly, SD-OCT images were captured with simultaneous visualization of the fundus in the infrared channel ($\lambda = 820$ nm). For each eye, seven horizontal 30° × 5° high-resolution (1536 × 1536 pixels) B-scans, spaced 240 μm between each other and centered in the area of atrophy with an automatic real time (ART, also called averaging or overlapping) of 25 scans per B-scan to improve the signal-to-noise ratio, were obtained at each session. Additionally, a single, high-resolution B-scan with an ART of 100 was acquired when possible. The SD-OCT images captured the first day were selected as a reference, and therefore it was possible to acquire all follow-up exams at exactly the same location as in the baseline, given the eye-tracking capabilities of the instrument.

### Histology and Immunohistochemistry

Since OCT findings showed no significant differences between month 1 and 2, the end of the study and were killed 2 months postoperatively by an intravenous overdose of sodium pentobarbital (Dolethal; Vetoquinol SA, Lure, France). Eyes were enucleated and the cornea and the lens were removed. The eye cups were then fixed in 4% paraformaldehyde in 0.1 M phosphate buffer for 3 hours at room temperature. After fixation, the eye cups were cryoprotected in serial sucrose solution: 15% (1 hour), 20% (1 hour), and 30% (overnight) at 4°C. Tissue samples were finally mounted in optimal cutting temperature compound (OCT; Sakura, Kobe, Japan).

Transverse sections (16 μm) were cut on a cryostat (Microm), mounted directly onto Superfrost Plus slides (Fisher Scientific, Loughborough, UK), and processed for immunocytochemistry. For blocking nonspecific staining, sections were incubated in 10% normal donkey serum for 30 minutes with 0.5% Triton X-100 and then incubated overnight at room temperature with several combinations of different primary antibodies, rhodopsin, JH455, recoverin, calbindin, calretinin, parvalbumin, and protein kinase C (PKC) alpha, against tight junctions of RPE, rods, cones, horizontal cells, bipolar cells, and amacrine and ganglion cells diluted in phosphate buffer (PB) 0.1 M, pH 7.4, plus 0.5% Triton X-100 (Table 1).

Following removal of the primary antibody, slides were incubated for 1 hour at a 1:100 dilution at room temperature in the corresponding secondary antibodies labeled with Alexa Fluor 488 (green), Alexa Fluor 555 (red), Alexa Fluor 633 (far red), or Alexa Fluor 647 (far red). Hoechst nuclear stain (H33342; Life Technologies, Grand Island, NY, USA) was used for the fluorescent labeling of cell nuclei. Slides were then mounted in antifade medium, and fluorescence was detected with a confocal laser scanning microscope (Leica Microsystems, Wetzlar, Germany). To make photomontages, each stack of images was aligned with the aid of Adobe Photoshop CS5 (Adobe Systems, Mountain View, CA, USA). Contralateral eyes were used as controls.

## RESULTS

### Postoperative Follow-Up Results

Results are depicted in Table 2. Spontaneous resolution of the subretinal bleb was observed in all the animals. Apart from pig 8, no significant anterior segment findings or elevated intraocular pressure was observed during the study period.

While pigs 1 (0.0005 mg/mL) and 2 (0.005 mg/mL) showed no fundus changes, pigs 3 and 4 (0.05 mg/mL, both) showed well-demarcated round lesions and pigmentary changes located at the area of the resolved blebs at 1-month fundus examination (Fig. 1). In these latter two animals, SD-OCT revealed marked atrophy and thinning of all the retinal layers at the center of the induced lesion. The RPE did not appear to be markedly attenuated, although it showed increased hyperreflectivity at the band corresponding to the junction of the outer segments and RPE, and increased hypertransmission of the signal into the choroid (Fig. 2).

Funduscopic pigmentary changes were even more evident in pigs 5 and 6 (0.5 mg/mL, both) 1 month postoperatively. Spectral-domain OCT changes were similar to those seen in pigs 1 and 2 but more severe, and the outermost hyperreflective bands showed hyperrreflectivity, irregularity, areas of attenuation, and disappearance of the band corresponding to

FIGURE 2. Spectral-domain OCT scan at 1 month at the area of lesion after subretinal administration of 0.1 mL $NaIO_3$ at concentration of 0.05 mg/mL in pig 4, demonstrating thinning and damage of all retinal layers, with thinning, irregularity, and discontinuity of the most external hyperreflective bands corresponding to the interdigitation zone and the RPE–Bruch's membrane complex. Increased transmission of the OCT signal into the choroid is also seen. *Red arrow* marks border of atrophy.

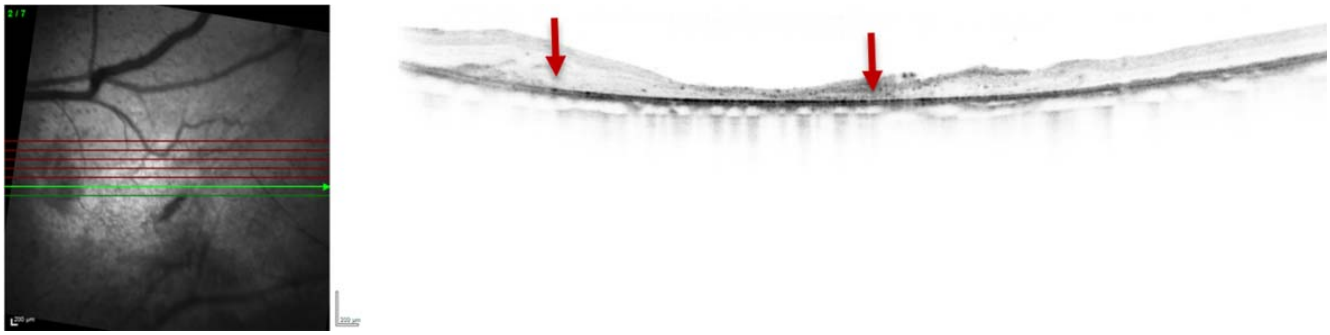

FIGURE 3. Spectral-domain OCT scan at 1 month at the area of lesion after subretinal administration of 0.1 mL $NaIO_3$ at concentration of 1 mg/mL in pig 7, demonstrating thinning and damage of all retinal layers, and more pronounced thinning and discontinuity of the most external hyperreflective bands compared to lower doses. Increased transmission of the OCT signal into the choroid is also seen. *Red arrow* marks border of atrophy.

the interdigitation zone, as well as increased hypertransmission of the signal into the choroid on SD-OCT.

In order to look for complete damage of the RPE layer, doses of 1 mg/mL (a ×2 dose of the initial solution) and of 3 mg/mL (a ×6 dose of the initial solution) were evaluated in pigs 7 and 8, respectively. Pig 7 showed at SD-OCT very severe atrophy and thinning of all retinal layers, including the RPE, with discontinuity and irregularity of the interdigitation band (Fig. 3). Unfortunately, pig 8 showed severe panuveitis 24 hours postoperatively and was humanely euthanized.

Since severe disruption seen by SD-OCT of the RPE was observed at doses that caused unselective marked damage of all retinal layers, the next goal was to look for a dose that would cause selective damage to the outer nuclear layer with preservation of the innermost retinal layers, including the outer plexiform layer, to better mimic the findings of SD-OCT

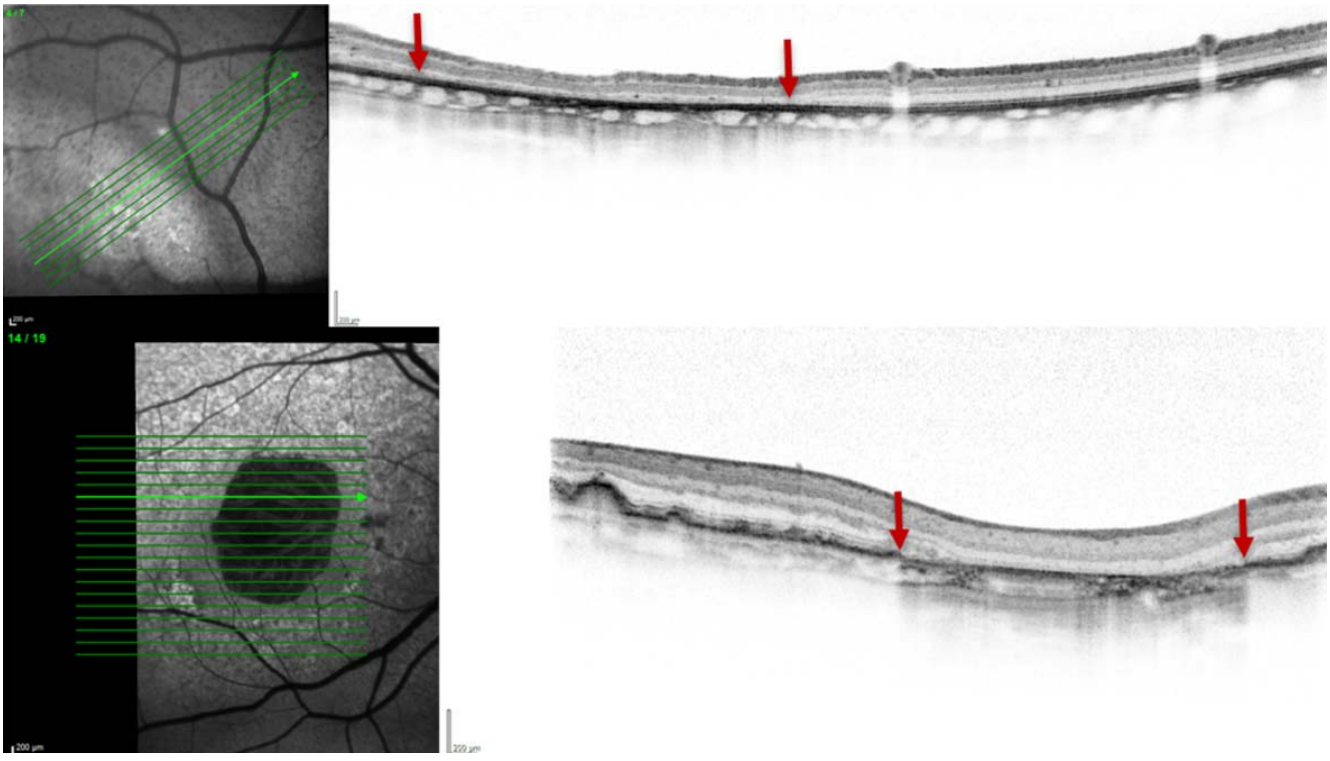

FIGURE 4. (**A**) (*top*) Spectral-domain OCT scan at 2 months at the area of lesion after subretinal administration of 0.1 mL $NaIO_3$ at concentration of 0.01 mg/mL in pig 12, demonstrating selective damage of the outer layers. A well-defined distinct transition zone is observed between nonaffected retina and damaged retina, where the outer nuclear layer and the ellipsoid zone disappear progressively. The inner nuclear layer is preserved and continuous over the entire lesion. The outer plexiform layer appears preserved in at least some areas, and the inner nuclear layer is lying directly over Bruch's membrane and residual RPE debris. Inner plexiform, ganglion cell, and nerve fiber layer appear to be unchanged. At the level of the retinal pigment epithelium there is increased reflectivity of the outer bands, interdigitation zone, and RPE–Bruch's complex, with irregularities and discontinuities. Increased transmission of the OCT signal into the choroid is visible under the lesion area. In contrast to the human SD-OCT scan, the external limiting membrane is not visible. (**B**) (*bottom*) Typical SD-OCT scan of a patient with GA secondary to AMD, showing well-demarcated edges between the atrophy and the preserved retina outside the boundaries. The outer nuclear layer, the external limiting membrane, and the ellipsoid zone progressively disappear at the transition zone. The outer plexiform layer appears preserved at least in some areas, and inner nuclear layer lying directly over Bruch's membrane and residual materials of the RPE. The inner plexiform, ganglion cell, and nerve fiber layer appear to be preserved. Increased transmission is clearly seen under the area of atrophy. *Red arrows* mark the borders of atrophy.

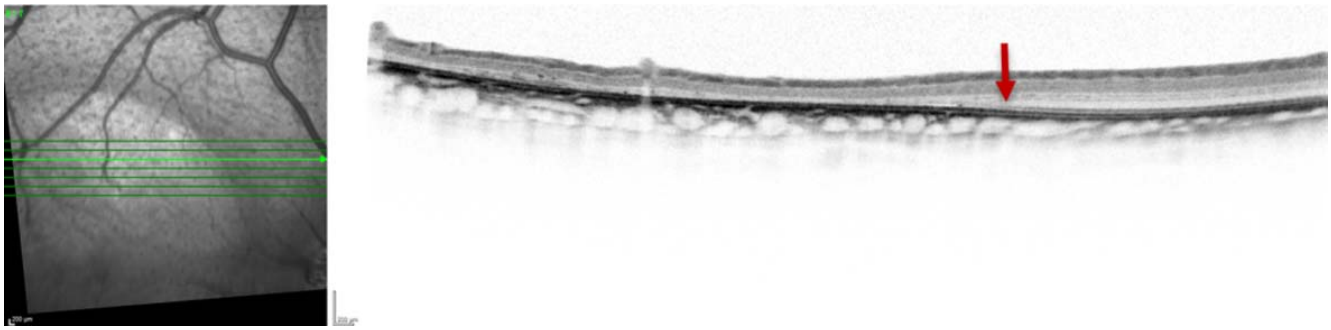

**Figure 5.** Spectral-domain OCT scan at 2 months at the area of lesion after subretinal administration of 0.1 mL $NaIO_3$ at concentration of 0.01 mg/mL in animal 15, showing the same results as the first animal using 0.01 mg/mL. Well-defined, circumscribed areas of selective damage of the outer layers are visible. As in humans, the outer plexiform layer and inner nuclear layer lie directly over the damaged RPE. *Red arrow* marks border of atrophy.

in patients with GA secondary to AMD. For this purpose, pigs 9 and 10 received 0.025 mg/mL (a dilution of 1/20) and pigs 11 and 12 received 0.01 mg/mL (a dilution of 1/50). Unfortunately, pig 11 died in the anesthetic recovery time, for reasons unrelated to the study. In pigs 9, 10, and 12, the SD-OCT lesions were more selective, involving only the external retinal layers, pig 12 being the one that showed better preservation of the outer plexiform layer. The SD-OCT findings in pig 12 (Fig.

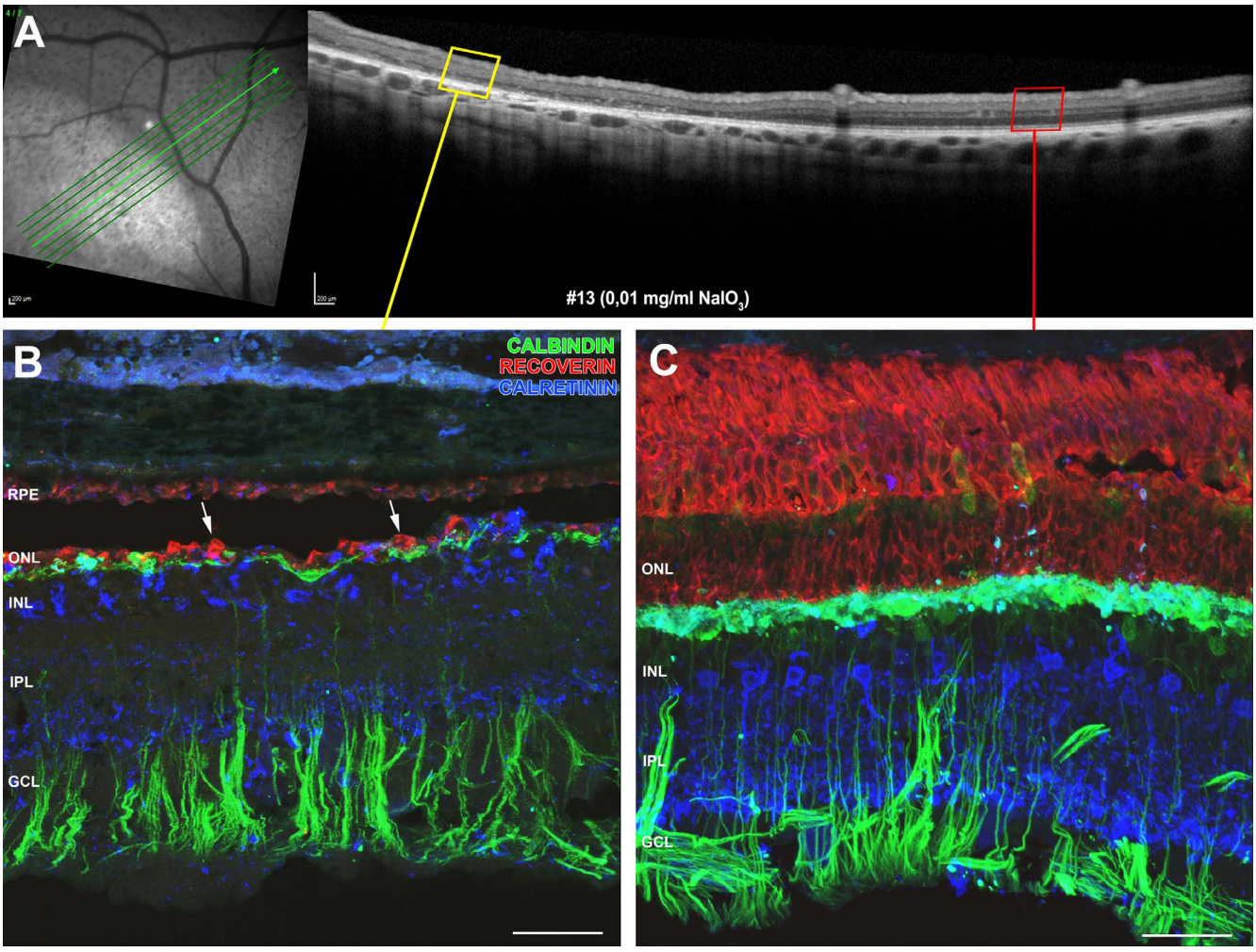


**Figure 6.** Spectral-domain OCT and histologic findings of 0.01 mg/mL subretinal sodium iodate in pig 13. (**A**) Spectral-domain OCT transverse image of the retina showing the area where the subretinal $NaIO_3$ was injected. (**B**, **C**) Confocal images taken at the location of the *yellow* (**B**) and *red* (**C**) squares shown at *right* in Figure 7A, corresponding to an area within the lesion and an area outside the lesion, on intact retina. In (**B**), recoverin immunolabeling (*red*) revealed a disorganized photoreceptor layer (*white arrows*), whereas the inner retina (calbindin in *green* and recoverin in *blue*) was intact morphologically. Image (**C**) revealed normal retinal layers. ONL, outer nuclear layer; INL, inner nuclear layer; IPL, inner plexiform layer; GCL, ganglion cell layer. *Scale bars*: 200 μm (**A**), 40 μm (**B**, **C**).

Investigative Ophthalmology & Visual Science

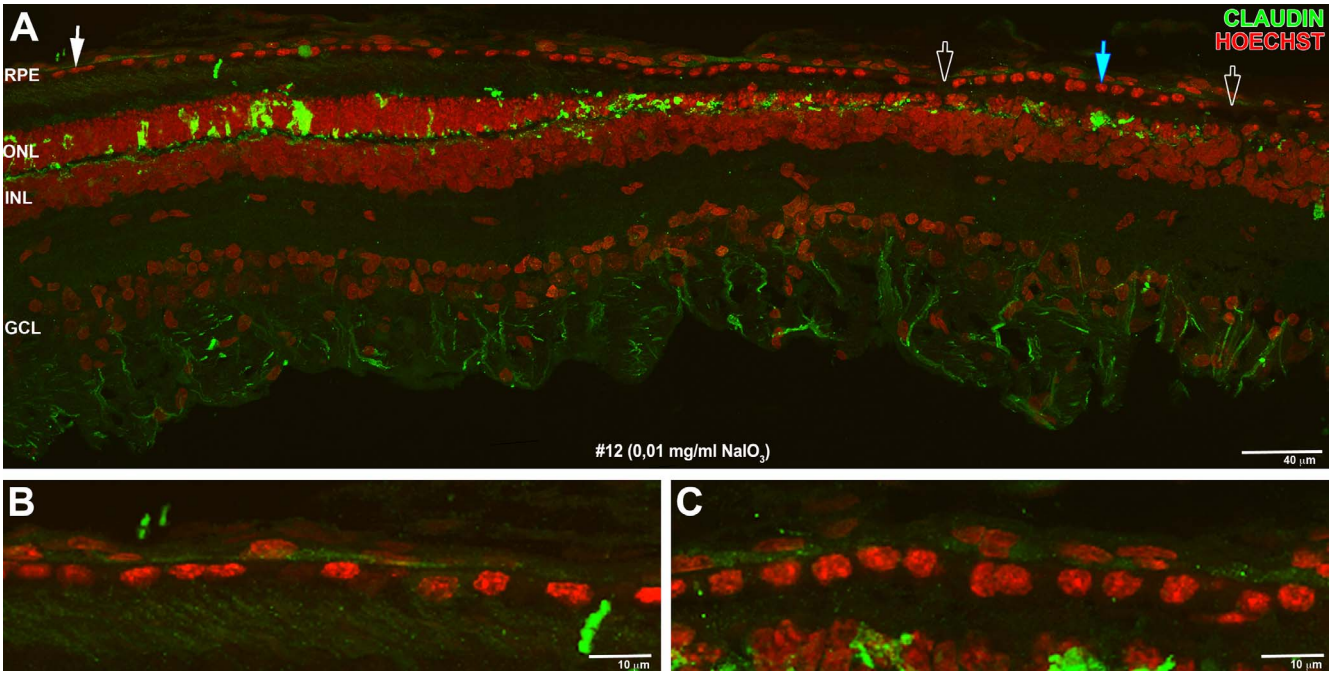


FIGURE 7. Immunohistochemical staining of a representative retina within a zone of the lesion induced with 0.01 mg/mL $NaIO_3$ in pig 12. (**A**) Labeling with claudin-1 (*green*) to detect blood–retinal barriers; Hoechst (*red*) denotes the progressive disappearance of the outer nuclear layers, especially at the transition zone (*blue arrow*). RPE layer is present in the two zones (*white and blue arrow*) but shows some irregularity and discontinuity (*white empty arrows*) in the lesion area. (**B**) Higher magnification of RPE (*white arrow* in [**A**]) shows normal architecture. (**C**) Detail of the morphologic changes in RPE at the atrophic area (*blue arrow* in [**A**]). Note that RPE nuclei are significantly bigger and more rounded in the lesion area. RPE, retinal pigment epithelium; ONL, outer nuclear layer; INL, inner nuclear layer; IPL, inner plexiform layer; GCL, ganglion cell layer. *Scale bars*: 40 µm (**A**); 10 µm (**B**, **C**).

4A) very closely resembled those observed in human patients suffering from GA secondary to AMD (Fig. 4B). Pigs 13, 14, and 15 also received 0.01 mg/mL to confirm, validate, and reproduce the findings observed in pig 12. These three pigs showed mild pigmentary changes at the area of the resolved induced bleb by indirect ophthalmoscopy, and selective damage and atrophy of the outer nuclear layer, with apparent preservation of the remaining inner retinal layers including the outer plexiform layer, by SD-OCT (Fig. 5). Spectral-domain OCT changes in all animals were already present at the month 1 examination and showed no significant changes at the month 2 examination.

### Histology and Immunocytochemistry Results

The histology of pigs receiving the dose of 0.01 mg/mL demonstrated well-demarcated lesions with a clear atrophy of the outer layers of the retina in the areas of the induced GA. The number of photoreceptors decreased considerably from the transition zone to the center of the lesion, where there were practically no photoreceptors, although the inner retina layers were well preserved (Fig. 6). Retinal pigment epithelium showed discontinuities and irregularities in the layer and changes in cell morphology, such as bigger and more rounded nuclei of the RPE. There was also a significant progressive decrease in claudin-1 expression in the outer retina within the GA zone (Fig. 7). This marker belongs to a family of transmembrane proteins that form junctional strands and are strongly related to the permeability and selectivity of tight junctions and expressed in intact blood vessels of mammalian retina and around RPE cells.[36] Similar findings with selective damage of the outer retinal layers and preservation of inner layers from the plexiform layer were also observed with hematoxylin and eosin staining at the dose of 0.01 (Fig. 8).

With doses $< 1$ mg/mL, no animal showed significant anterior or posterior inflammation in the early or late postoperative follow-up. No abnormal intraocular pressure readings were observed.

Spontaneous resolution of the subretinal bleb and absence of retinal detachment were observed in all animals using the 38-gauge subretinal cannula, despite neither vitrectomy nor posterior vitreous detachment being performed in any animal. No animal developed cataract during the postoperative period.

## DISCUSSION

A major difficulty in the research on therapies for GA is the lack of good animal models.[37] This is either because they do not show features similar to GA or because of a lack of similarities between the animal and the human being in terms of anatomy and physiology. This is especially true for models in large animals.

In advanced cases of GA, there is a need for a regenerative treatment rather than a treatment to stop progression. Thus, in order to achieve an ideal regenerative treatment, there is an unmet need to obtain a large animal model that would mimic the GA characteristics and in which evolving therapies could be used to test their efficacy. Furthermore, Stargardt's disease, another form of GA of the outer layers with certain similarities to GA, has a severe functional cost in young patients, with a huge emotional and socioeconomic impact for them and their relatives.

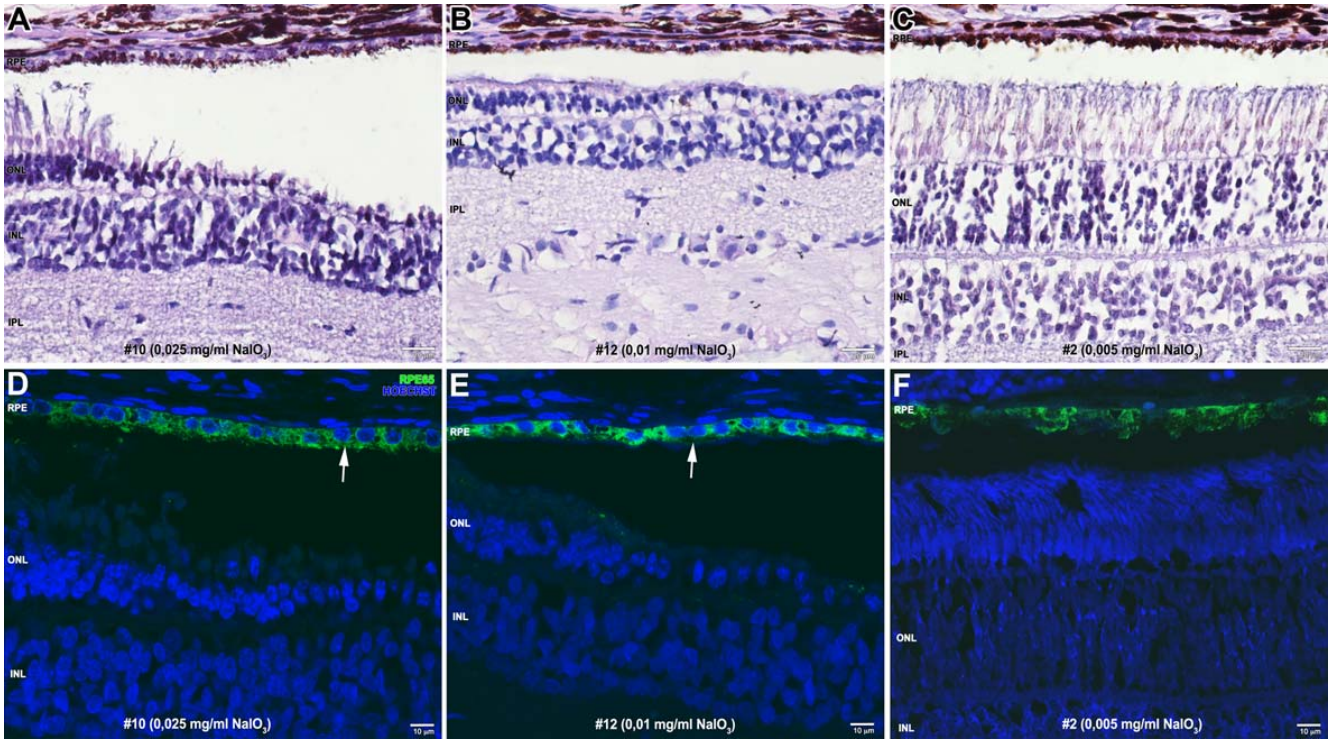


**Figure 8.** Hematoxylin and eosin (**A**–**C**) and RPE65 (**D**–**F**) staining. In (**A**), the transition from damaged retina to the preserved retina is observed with a dose of 0.025 mg/mL in pig 10. Outer nuclear layer and outer and inner segments are progressively present beyond this junction zone. (**B**) Selective damage of outer retinal layers within the induced lesion with a dose of 0.01 mg/mL in pig 12. (**C**) No evident histologic changes are visible with low doses of 0.005 mg/mL as in pig 2. (**D**, **E**) RPE65 immunostaining close to the transition zone, showing bigger and more rounded nuclei of the RPE cells with smaller cell cytoplasm both with doses of 0.025 and 0.01 mg/mL in animals 15 and 12 (*white arrows*). At lower doses of 0.005 mg/mL as in pig 2, no visible changes are evident at the RPE level. RPE, retinal pigment epithelium; ONL, outer nuclear layer; INL, inner nuclear layer; IPL, inner plexiform layer. *Scale bars*: 20 μm (**A**–**C**); 10 μm (**D**–**F**).

Although enormous progress has been made in the field of pathogenesis of AMD, it is still an extremely complex disease with many unresolved questions. Any AMD animal model development is particularly challenging, as the causative agent, the genetic link, and the mechanism of AMD are not well known.

The production of this porcine model has many advantages: It is a rapid and simple procedure, easily reproducible and relatively not iatrogenic, as vitrectomy is not performed as part of the toxin-induced atrophy procedure. In addition, a relatively large number of animals with resulting atrophy can be generated in order to fulfill the requirements of any study in a short time. However, the major advantage is the possibility of having a model of circumscribed, well-defined damage of the outer layers only, well demonstrated and reproducible by SD-OCT. This may be very useful to test regenerative therapies in which indemnity of inner layers is needed (i.e., optogenetics) and in which indemnity of choriocapillaris, RPE, and retina in the vicinity is needed in order for cell therapy approaches to have a relatively close-by preserved environment for a greater chance to settle.

The minimally invasive procedure (e.g., no vitrectomy, no posterior vitreous detachment, no cataract induction) allows additional interventions such as stem cell implantation with minimal influences from the initial procedure of the atrophy induction. The relatively fast and stable atrophy induction that occurs as soon as 30 days after the procedure permits the performance of posterior therapeutic or experimental interventions in a relatively short period, minimizing the long-term follow-up needed in these animals for the entire procedure. It is clear, however, that using minipigs would ease the management of these animals beyond month 3 due to the growth and weight increase in the animals used in this study, especially if further interventions testing therapies are to be performed.

The main endpoint used in this model was the features of circumscribed, well-defined selective damage of outer retinal layers with preservation of the inner retinal layers from outer plexiform layer, observed by SD-OCT and posteriorly confirmed and correlated with the histology, in order to resemble the outer retinal layer atrophy seen in GA secondary to AMD. Surprisingly, RPE appeared to be more resistant than the photoreceptors. Whenever dosing of subretinal $NaIO_3$ was increased in order to obtain visible complete damage by SD-OCT of the RPE, the selectivity of outer layer atrophy was lost. Therefore, we focused on the search for the optimal dosing to damage the outer layers while preserving the inner layers. The dose of 0.01 mg/mL (the dilution of 1/50) appeared to be the ideal one, and this was confirmed in additional animals. Although SD-OCT did not show evident complete damage to the RPE at the areas of atrophy, irregularities, discontinuities, and increased hyperreflectivity of the two outermost bands (the interdigitation zone and the RPE/Bruch's membrane complex), in addition to loss of the ellipsoid zone, were observed. Increased transmission of the signal into the choroid was also present, a typical OCT feature of RPE atrophy in humans with GA secondary to AMD. The histologic results confirmed the OCT findings showing damage at the level of the layers similar to those observed in GA-AMD. Immunocytochemistry showed a significant decrease in expression of claudin, which is a family of transmembrane proteins that form junctional strands and are strongly related with the permeabil-

ity and selectivity of tight junctions, confirming that RPE is damaged in this model in addition to the selective damage of the outer nuclear layer.

To the authors' knowledge, this is the first study to create a useful validated SD-OCT porcine toxin-induced model of a controlled area of circumscribed retinal damage, with well-delimited borders and selectively of the outer layers of the retina, mimicking GA in AMD, which assimilates most features of the human disease and was confirmed by immunocytochemistry.

Despite the previously mentioned advantages, some drawbacks should be emphasized. This model is toxic and not genetically induced and neither related to an aging process nor developed in aged animals, and therefore will not show progression of the atrophic lesion. Also, although SD-OCT findings showed no significant changes from the month 1 to month 2 examinations, further studies with longer follow-up and in minipigs would be ideal. Despite these drawbacks, this model may represent a leap in terms of better understanding the GA process formation and especially the behavior of experimental regenerative approaches.

In summary, the large animal model validated herein by both SD-OCT and immunocytochemistry presents several clinical and histologic features of GA AMD. Therefore, it may represent a valuable tool in the investigation of new emerging regenerative therapies that aim to restore visual function, such as retinal or stem cell transplantation, or optogenetics. Spectral-domain OCT validation may allow follow-up evaluation of the aforementioned therapies performed in these animals in vivo, in order to mimic the current gold standard clinical imaging follow-up in human patients under these emerging experimental regenerative approaches.

## *Acknowledgments*

Supported by Barcelona Macula Foundation, Barcelona, Spain, and Departament de Medicina i Cirurgia Animals, Facultat de Veterinària, Universitat Autònoma de Barcelona, Barcelona, Spain.

Disclosure: **J. Monés**, None; **M. Leiva**, None; **T. Peña**, None; **G. Martínez**, None; **M. Biarnés**, None; **M. Garcia**, None; **A. Serrano**, None; **E. Fernandez**, None

## *References*

1. Michels S, Rosenfeld PJ, Puliafito CA, Marcus EN, Venkatraan AS. Systemic bevacizumab (Avastin) therapy for neovascular age-related macular degeneration: twelve-week results of an uncontrolled open-label clinical study. *Ophthalmology*. 2005; 112:1035–1047.
2. Rosenfeld PJ, Brown DM, Heier JS, et al. Ranibizumab for neovascular age-related macular degeneration. *N Engl J Med*. 2006;355:1419–1431.
3. Brown DM, Kaiser PK, Michels M, et al. Ranibizumab versus verteporfin for neovascular age-related macular degeneration. *N Engl J Med*. 2006;355:1432–1444.
4. Kaiser PK, Brown DM, Zhang K, et al. Ranibizumab for predominantly classic neovascular age-related macular degeneration: subgroup analysis of first-year ANCHOR results. *Am J Ophthalmol*. 2007;144:850–857.
5. Brown DM, Michels M, Kaiser PK, et al. Ranibizumab versus verteporfin photodynamic therapy for neovascular age-related macular degeneration: two-year results of the ANCHOR study. *Ophthalmology*. 2009;116:57–65, e5.
6. Schmidt-Erfurth U, Kaiser PK, Korobelnik JF, et al. Intravitreal aflibercept injection for neovascular age-related macular degeneration: ninety-six-week results of the VIEW studies. *Ophthalmology*. 2014;121:193–201.
7. Klein R, Klein BE, Knudtson MD, Meuer SM, Swift M, Gagnon RE. Fifteen-year cumulative incidence of age-related macular degeneration: the Beaver Dam Eye Study. *Ophthalmology*. 2007;114:253–262.
8. Augood CA, Vingerling JR, de Jong PT, et al. Prevalence of age-related maculopathy in older Europeans: the European Eye Study (EUREYE). *Arch Ophthalmol*. 2006;124:529–535.
9. Brown GC, Brown MM, Sharma S, et al. The burden of age-related macular degeneration: a value-based medicine analysis. *Trans Am Ophthalmol Soc*. 2005;103:173–184.
10. Brown GC, Lieske HB, Lieske PA, Brown K. The economics of age-related macular degeneration. In: Ho AC, Regillo CD, eds. *Age-Related Macular Degeneration: Diagnosis and Treatment*. New York: Springer; 2011:155–173.
11. Holz FG, Bellman C, Staudt S, Schütt S, Völker HE. Fundus autofluorescence and development of geographic atrophy in age-related macular degeneration. *Invest Ophthalmol Vis Sci*. 2001;42:1051–1056.
12. Vinding T. Age-related macular degeneration. Macular changes, prevalence and sex ratio. An epidemiological study of 1000 aged individuals. *Acta Ophthalmol*. 1989;67:609–616.
13. Klein R, Klein BE, Linton KL. Prevalence of age-related maculopathy. The Beaver Dam Eye Study. *Ophthalmology*. 1992;99:933–943.
14. Ferris FL III, Fine SL, Hyman L. Age-related macular degeneration and blindness due to neovascular maculopathy. *Arch Ophthalmol*. 1984;102:1640–1642.
15. Martin DF, Maguire MG, Ying GS, et al. Ranibizumab and bevacizumab for neovascular age-related macular degeneration. *N Engl J Med*. 2011;364:1897–1908.
16. Sunness JS, Gonzalez-Baron J, Applegate CA, et al. Enlargement of atrophy and visual acuity loss in the geographic atrophy form of age-related macular degeneration. *Ophthalmology*. 1999;106:1768–1779.
17. Sunness JS, Rubin GS, Broman A, Applegate CA, Bressler NM, Hawins BS. Low luminance visual dysfunction as a predictor of subsequent visual acuity loss from geographic atrophy in age-related macular degeneration. *Ophthalmology*. 2008;115: 1480–1488.
18. Owsley C, Jackson GR, Cideciyan AV, et al. Psychophysical evidence for rod vulnerability in age-related macular degeneration. *Invest Ophthalmol Vis Sci*. 2000;41:267–273.
19. Curcio CA, Millican CL, Alen KA, Kalina RE. Aging of the human photoreceptor mosaic: evidence for selective vulnerability of rods in central retina. *Invest Ophthalmol Vis Sci*. 1993;34:3278–3296.
20. Curcio CA, Medeiros NE, Millican CL. Photoreceptor loss in age-related macular degeneration. *Invest Ophthalmol Vis Sci*. 1996;37:1236–1249.
21. Jackson GR, Owsley C, Curcio CA. Photoreceptor degeneration and dysfunction in aging and age-related maculopathy. *Ageing Res Rev*. 2002;1:381–396.
22. Scholl HP, Bellman C, Dandekar SS, Bird AD, Fitzke FW. Photopic and scotopic fine matrix mapping of retinal areas of increased fundus autofluorescence in patients with age-related maculopathy. *Invest Ophthalmol Vis Sci*. 2004;45:574–583.
23. Chen C, Wu L, Wu D, et al. The local cone and rod system function in early age-related macular degeneration. *Doc Ophthalmol*. 2004;109:1–8.
24. Edwards AO, Malek G. Molecular genetics of AMD and current animal models. *Angiogenesis*. 2007;10:119–132.
25. Pennesi ME, Neuringer M, Courtney RJ. Animal models of age related macular degeneration. *Mol Aspects Med*. 2012;33:487–509.
26. Ambati J, Ambati JK, Yoo SH, Ianchulev S, Adamis AP. Age-related macular degeneration: etiology, pathogenesis, and therapeutic strategies. *Surv Ophthalmol*. 2003;48:257–293.

27. Kiilgaard JF, Prause JU, Prause M, Scherfig E, Nissen MH, la Cour M. Subretinal posterior pole injury induces selective proliferation of RPE cells in the periphery in in vivo studies in pigs. *Invest Ophthalmol Vis Sci*. 2007;48:355–360.
28. Sanchez I, Martin R, Ussa F, Fernandez-Bueno I. The parameters of the porcine eyeball. *Graefes Arch Clin Exp Ophthalmol*. 2011;249:475–482.
29. Fauser S, Luberichs J, Schuttauf F. Genetic animal models for retinal degeneration. *Surv Ophthalmol*. 2002;47:357–367.
30. Hariri S, Moaued AA, Choh V, Bizheva K. In vivo assessment of thickness and reflectivity in a rat outer retinal degeneration model with ultrahigh resolution optical coherence tomography. *Invest Ophthalmol Vis Sci*. 2012;53:1982–1989.
31. Machalinska A, Lubinski W, Klos P, et al. Sodium iodate selectively injuries the posterior pole of the retina in a dose-dependent manner: morphological and electrophysiological study. *Neurochem Res*. 2010;35:1819–1827.
32. Franco LM, Zuliger R, Wolf-Schnurrbusch UE, et al. Decreased visual function after patchy loss of retinal pigment epithelium induced by low-dose sodium iodate. *Invest Ophthalmol Vis Sci*. 2009;50:4004–4010.
33. Korte GE, Gerszberg T, Pua F, Henkind P. Choriocapillaris atrophy after experimental destruction of the retinal pigment epithelium in the rat. A study in thin sections and vascular casts. *Acta Anat (Basel)*. 1986;127:171–175.
34. Noel JM, Fernandez de Castro JP, Demarco PJ Jr, et al. Iodoacetic acid, but not sodium iodate, creates an inducible swine model of photoreceptor damage. *Exp Eye Res*. 2012;97:137–147.
35. Hayasaka S, Noda S, Setogawa T. Effect of drugs in vitro on lysosomal enzyme activities in bovine retinal pigment epithelial cells. *Jpn J Ophthalmol*. 1988;32:316–321.
36. Morita K, Furuse M, Fujimoto K, Tsukita S. Claudin multigene family encoding four-transmembrane domain protein components of tight junction strands. *Proc Natl Acad Sci U S A*. 1999;96:511–516.
37. Holz FG, Schmitz-Valckenberg S, Fleckenstein M. Recent developments in the treatment of age-related macular degeneration. *J Clin Invest*. 2014;124:1430–1438.

Investigative Ophthalmology & Visual Science